applied sciences

MDPI

Article

Development of Deployable Reflector Antenna for the SAR-Satellite, Part 3: Environmental Test of Structural-Thermal Model

Hyun-Guk Kim, Dong-Geon Kim, Ryoon-Ho Do, Min-Ju Kwak, Kyung-Rae Koo and Youngjoon Yu *

Space R&D Center, Hanwha Systems, Gyeonggidong-ro, Namsa-eup, Cheoin-gu, Yongin-si 491-23, Gyeonggi-do, Republic of Korea; hyunguk1.kim@hanwha.com (H.-G.K.); dgkim90@hanwha.com (D.-G.K.); doable19@hanwha.com (R.-H.D.); kwakminj@hanwha.com (M.-J.K.); kr.koo@hanwha.com (K.-R.K.)
* Correspondence: youngjoon.yu@hanwha.com

Abstract: The concept of synthetic aperture radar (SAR) has the advantage of being able to obtain high-quality images even when the target area is at night or covered with obstacles such as clouds or fog. These imaging capabilities have led to a rapid increase in demand for space SAR imagery across a variety of sectors, including government, military, and commercial sectors. The SAR-based deployable reflector antenna was developed in this series of paper. The satellite performance is influenced by the aperture size of an antenna. To improve the image acquisition performance, the SAR antenna has the configuration of several foldable CFRP reflectors. In this paper, the experimental investigation of the Structural-thermal model deployable reflector antenna is performed. During the launch condition, the satellite and payload are subjected to the dynamic load. In the STM phase, the acoustic test was conducted to evaluate the structural stability of the deployable reflector antenna within the acoustic environment. The sinusoidal vibration test was implemented to investigate the fundamental frequency for inplane/normal directions and evaluate the structural stability of reflector antenna. By using experimental data obtained from the thermal-balance test, the well-correlated thermal analysis model was established to execute the orbital thermal analysis. The experimental results of the environmental test in STM phase show that the deployable reflector antenna has structural stability for the structural/thermal environments. The configuration of the deployable reflector antenna determined in STM phase can be applied to the qualification model.

Keywords: deployable reflector antenna (DR-A); structural-thermal model (STM); environment test; sinusoidal vibration test; acoustic load test; thermal-balance test

check for updates

Academic Editor: Atsushi Mase

Received: 26 December 2024
Revised: 20 January 2025
Accepted: 24 January 2025
Published: 30 January 2025

Citation: Kim, H.-G.; Kim, D.-G.; Do, R.-H.; Kwak, M.-J.; Koo, K.-R.; Yu, Y. Development of Deployable Reflector Antenna for the SAR-Satellite, Part 3: Environmental Test of Structural-Thermal Model. *Appl. Sci.* **2025**, *15*, 1436. https://doi.org/10.3390/app15031436

Copyright: © 2025 by the authors. Licensee MDPI, Basel, Switzerland. This article is an open access article distributed under the terms and conditions of the Creative Commons Attribution (CC BY) license (https://creativecommons.org/licenses/by/4.0/).

1. Introduction

Synthetic aperture radar (SAR), proposed in the 1960s is able to obtain high-quality images regardless of day/night or whether condition of the target area [1,2]. Due to this image acquisition performance, the demand for SAR imaging technology is rapidly increasing in various sectors including government, military, and commercial sectors [3,4]. In general, the image acquisition performance of a satellite antenna is determined by the dimension of the antenna aperture, because the antenna transmits electromagnetic waves and receive backscattered signals from the target object. However, SAR-based antennas are mounted on a moving platform and receive backscattered signals at a moving location, the distance between the original and new position make a virtual antenna size that is wider than the size of the physical antenna. Therefore, the SAR-based antenna is advantageous to

obtain the precise satellite image. Because the diameter of the physical antenna is also very important, the configuration of the satellite antenna should be the deployable configuration that is launched in the fairing of a limited volume. This type of antenna has the advantage of having high storage efficiency because it may be loaded in a storage state even in physically limited projectile pairing [5–8].

Several studies have been conducted to develop a deployable reflector antenna. In 1999, Thomson proposed a ring-truss type of deployable mesh antenna [9]. In 2003, Meguro et al. proposed the beam steering method of mesh antenna and performed experimental verification for the beam steering performance [7]. In addition, Sun et al. designed and verified the deployment mechanism of the ring-truss type mesh antenna numerically and experimentally [8]. The mesh antenna studied in the above three literatures can be used in the satellite antenna with a large diameter relative to its weight, but has the low stiffness property of the reflective surface, it is possible to cause relatively high surface error. The high surface error of the mesh antenna deteriorates the quality of satellite images, and the low dynamic stiffness causes a problem of delaying the photographing preparation time by causing large vibrations during the attitude controls [10]. From this point of view, it is necessary to develop a solid type deployable reflector antenna using a CFRP honeycomb sandwich structure [11,12].

The deployable reflector antennas require high reliability for not only the deployment mechanism in the orbital environment but also the restriction force for the stowed condition in the launch environment. The deployable reflector antenna proposed in the series of papers is operated by the deployment mechanism with the constant force spring (CFS) of the hinge part in the orbital environment and maintains the stowed condition by the hold-and-release synchronizing mechanism (HRSM) at the top and the hold-and-release belt mechanism (HRBM) in the middle. Therefore, the three types of the hold-and-release mechanisms consisting of metallic material and the main reflector and main structure, which are composite material should ensure structural stability for the launch environment.

Satellites are subjected to the high-level dynamic loads during the launch process. During the launch process, the combustion noise of the launch vehicle is reflected on the ground surface and transmitted into the launch vehicle, and the flow-induced noise caused by friction between the outer surface of the launch vehicle and the air is also transmitted into the fairing of the launch vehicle. This noise creates a severe reverberation sound field inside the fairing in the vehicle. In addition, this wideband air-born noise creates random vibrations in the satellite and payload. Because of the pitch maneuver to enter the mission orbit, the launch vehicle experiences a periodic load due to the fuel injection cycle of the sub engine. This periodic load causes a sinusoidal load on the satellite and payload. In order to evaluate the structural stability of the satellite/payload, an experimental verification process is required at the structural-structural model (STM) phase for the acoustic/vibration loads. Also, the satellites that enter the mission orbit are exposed to severe thermal environment as the satellite operates between the Earth and the Sun at regular intervals during the mission life. Therefore, orbital thermal analysis should be implemented to confirm the temperature range of the satellite/payload. Before performing orbital thermal analysis, the material properties of the thermal analysis model and the thermal conductivity coefficient between components must be corrected, and the temperature data for the model correction must be experimentally obtained to be used in the correlation of the thermal analysis model.

In this study, the sine vibration tests and acoustic load tests are performed to verify the structural stability of the STM of the deployable reflector antenna under the dynamic loads in the launch environment. In addition, the temperature data for constructing the orbital thermal analysis model was obtained from the thermal balance tests. Based on

the Environmental test performed in this paper, we confirm the detailed design of the deployable reflector antenna. These experimental results will be used in the qualification model (QM) phase.

2. An Overview of the Deployable Reflector Antenna Based on CFRP Honeycomb Sandwich Structure

Figure 1 shows the general development process of the satellite/payload. First of all, in the development model (DM) phase, the function and performance tests are performed on the partially simplified models from a mechanical perspective. For example, the DM phase includes the deployment of solar panels in orbit, verification of assembly, and specimen testing. In the structural-thermal model (STM) phase, the environmental tests are performed to evaluate the structural stability against the acoustic and vibrational loads. In the STM phase, the verification for the deployment mechanism is not required, because the satellite/payload should maintain the stowed condition in the launch environment. However, the center of gravity (CoG) of the STM needs to be aligned to mimic the mass properties of the real model. Therefore, in the STM stage, the hinge, synchronization, and belt mechanisms are designed by dummy structure without the functionality of the deployment. The qualification model (QM) is designed/manufactured reflecting the environmental results performed in the STM phase. The QM has the function/performance same with the flight model. The experimental verification in QM phase includes not only the several dynamic structural tests same with STM phase but also the thermal vacuum test for the orbital environment.

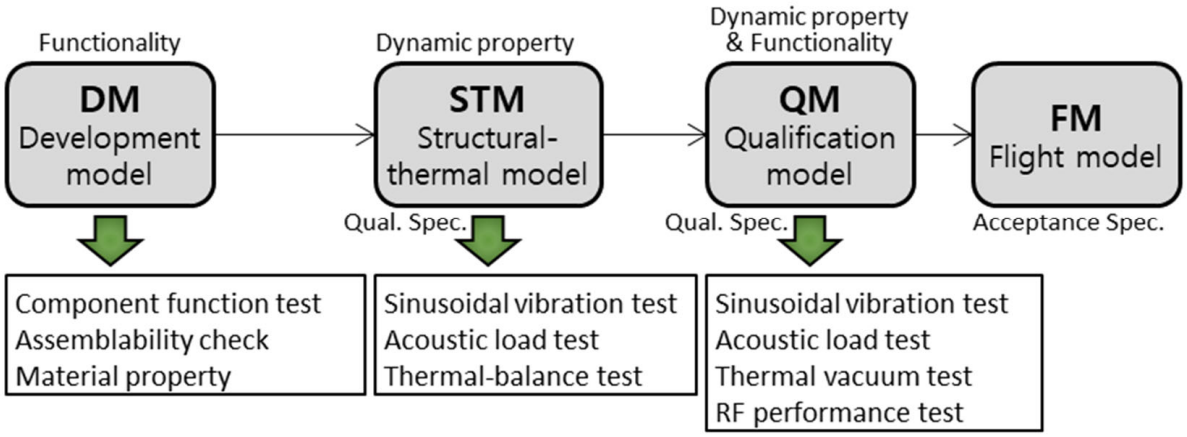


Figure 1. General flow chart for the development of the satellite/payload.

Figure 2 shows the deployable reflector antenna model under development. In previous papers of this series, we dealt with the design [5] and fabrication [13] of the main reflector composed of YSH70A [11], which is a space-grade carbon composite, and aramid core [12], which is a lightweight material. In this study, we manufacture the reflector antenna components including the main reflector, main structure, base plate and the three types of hold-and-release mechanism and integrate STM of the reflector antenna under the stowed condition. Finally, we performed the environmental test for the launch environment. The deployment mechanism structure (deployment, synchronizing, belt mechanism) of STM was developed as the dummy structure using Aluminum (AL6061) material, which does not provide a deployment functionality. The experimental results are used in the verification of structural stability for the vibration/acoustic load and the model correlation of the thermal analysis model of the antenna.

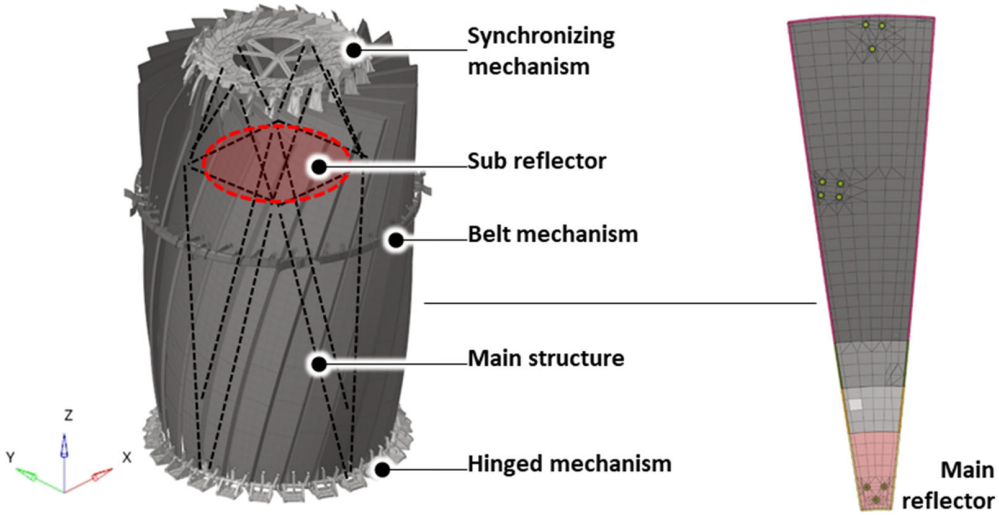


Figure 2. Conceptual diagram of the deployable reflector antenna in STM phase.

3. Sinusoidal Vibration Test of the Deployable Reflector Antenna in STM Phase

Figure 3 shows the test configuration and procedure of the sinusoidal vibration test at the STM phase. The sinusoidal vibration test is to evaluate the structural stability against the sinusoidal load propagated to the payload through launch adaptor during the launch process. Unlike the computer analysis that numerically calculates the acceleration response of each component according to the set test specifications, the test is started at a relatively low-level input load. And then, the input acceleration level is gradually increased to protect the reflector antenna prototype during the environmental test. The sinusoidal vibration test is performed for each of the x, y, and z axes in the test environment of Figure 3a–c, and the test procedure is as shown in Figure 3d. The sinusoidal vibration test starts at 1/3 level of the test specifications and is performed stepwise up to the full level-el test, and a low-level sine sweep test (LLSST) is performed before/after each step of the intermediate level to calculate the frequency and amplitude shift of the fundamental mode frequency. Two shift values are the pass/fail criteria of the sinusoidal vibration test. Generally, if the frequency and amplitude shift of the fundamental mode is more than 5% before/after each test, it is considered that there is a problem, such as a crack, loosening of a bolt or permanent deformation, with the test specimen [13]. The sinusoidal vibration test of the reflector antenna in STM phase was conducted with the dummy structure of X- and S-band antenna assembly located in the top side to express the structural behavior property of the reflector antenna.

Figure 4 shows the modal analysis of the deployable reflector antenna in the stowed condition. The antenna developed in this study is mounted to the satellite body using eight bolts on the base plate. As shown in Figure 4a, the analysis model of the reflector antenna connects the eight-bolting hole to a rigid body element, and a fixed boundary condition is imposed to the independent nodes of the rigid body element. Figure 4b,c shows that the vibration modes of the reflector antenna for the x and y directions are 24.6 Hz (2nd mode) and 24.5 Hz (1st mode), reflectively. The z-directional mode is 121.1 Hz (160th mode). Because the modal effective mass fraction of the vibration modes in Figure 4a–c is more than 0.5, three modes represent the dynamic behavior for each direction (inplane/out-of-plane). The out-of-plane vibration mode appears at a higher frequency band than the in-plane mode. It means that the reflector antenna has high dynamic stiffness in the out-of-plane direction.

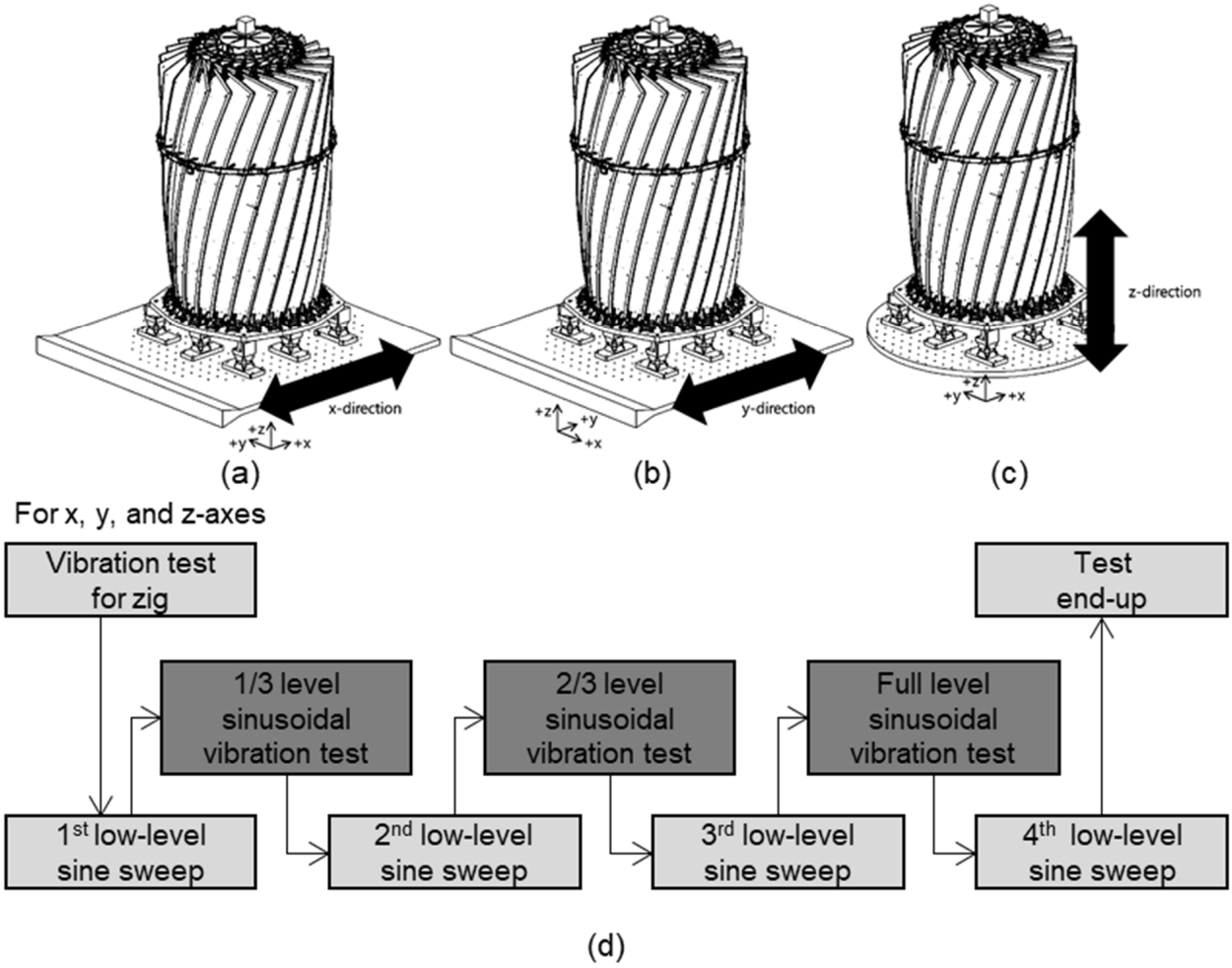


Figure 3. Concept of sinusoidal vibration test; the test configuration with vibration zig for (**a**) x, (**b**) y, and (**c**) z-axes and (**d**) test procedure.

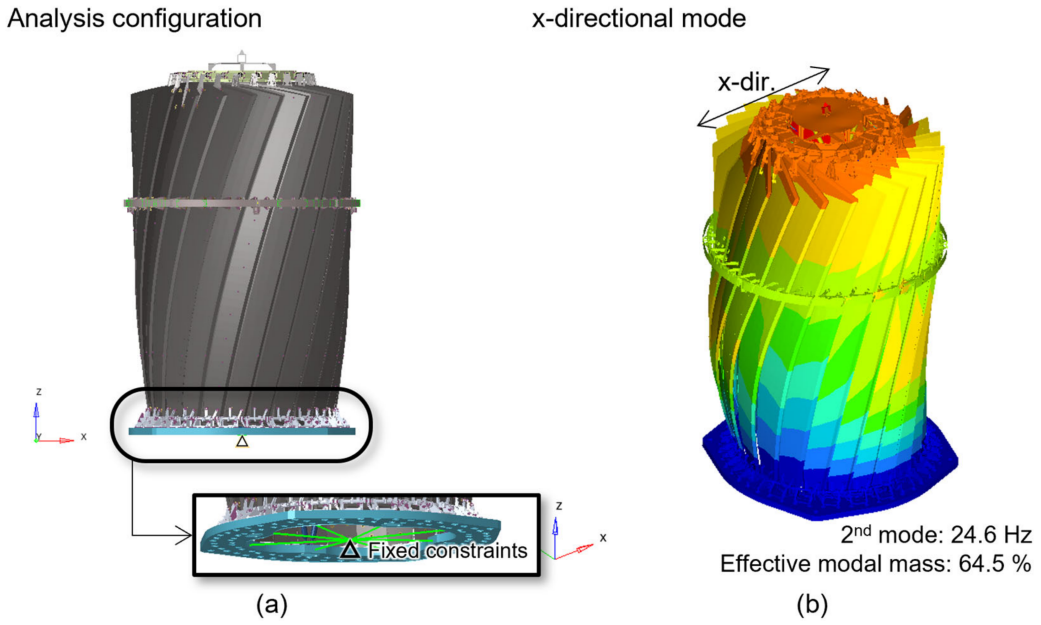


Figure 4. *Cont.*

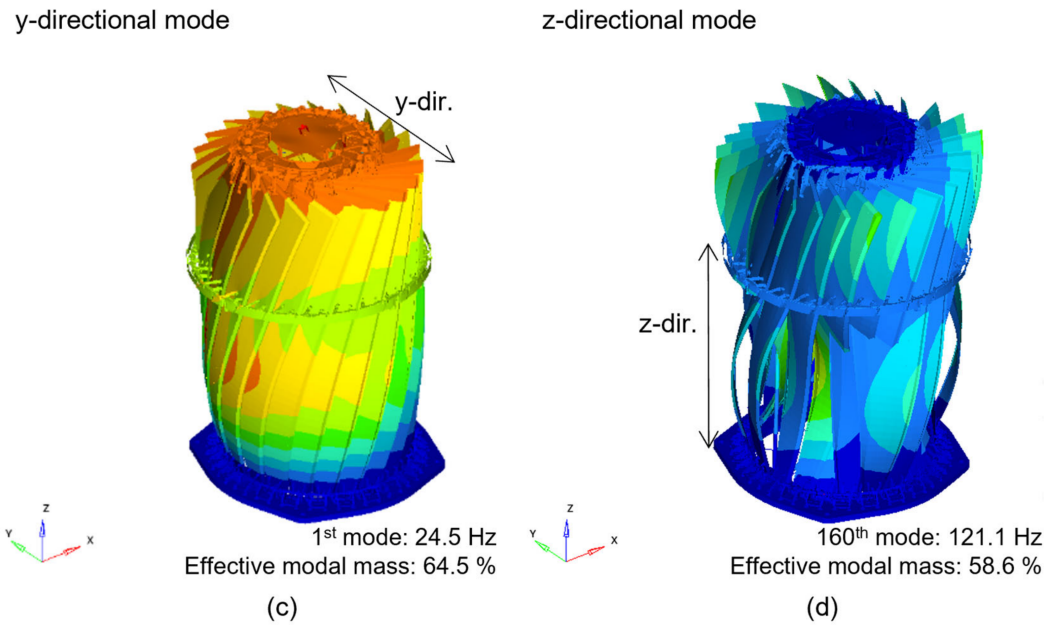


Figure 4. Modal analysis of the deployable reflector antenna under the stowed condition; (**a**) analysis configuration; analysis results of mode shapes, frequencies, and effective modal mass along (**b**) x-, (**c**) y-, and (**d**) z-axes, respectively.

Before the sinusoidal vibration test, the structural stability of the STM of the reflector antenna was evaluated by using the finite element analysis. Figure 5 shows the sinusoidal test configuration and result for the reflector antenna in STM phase. Figure 5a shows the test configuration of the sine vibration. As mentioned above, the bottom part of the reflector antenna is connected to the satellite body by eight bolts. The excitation forces in the in-plane and out-of-plane directions are as shown in the vibration specification in Figure 5b. As shown in Figure 5c, the test specification relaxation was applied to the sinusoidal vibration test for the in-plane direction. In the sinusoidal vibration test, a tri-axial load cell (Kistler type 9377C) with a calibrated range of −30 kN to 30 kN was used at eight interfaces to measure the interface load transmitted from the satellite body [14]. The maximum allowable load of the calibrated load range of the loadcell is 60 kN. Because the interface forces calculated from the original specification exceed the maximum allowable measuring force, the test specification for in-plane direction is reduced as the notched specification as shown in Table 1. For the out-of-plane direction, the interface load is not exceeding the calibrated range of the loadcell. The reason why the z-directional interface load is relatively small is that the CoG of STM is located near the center.

In the sinusoidal vibration test performed by the acceleration input profile of the notched specification, the interface load measured by the loadcell falls within the calibrated range. LLSST was performed before and after the intermediate level vibration test to evaluate the frequency and amplitude shift. LLSST, so-called modal searching, is a test that excites a wide frequency band at a relatively low and constant level to identify the vibration mode. Conventional LLSST has been performed in the frequency range of 5 to 2000 Hz. However, since the vibration modes for the in-plane and out-of-plane directions are 121.1 and 24.5 Hz, respectively, the frequency range of the LLSST performed in the sinusoidal test is the relatively narrow frequency range from 5 to 200 Hz. As shown in Figure 5c,d, the responses of the control accelerometer for the full level test show that the sinusoidal vibration test was performed satisfying the specifications defined in Table 1. In addition, Figure 5e and f show the comparison of the 1st to 4th LLSS results. The in-plane and out-of-plane modes calculated in Figure 4 show a frequency shift of less than 5% and

an amplitude shift of less than 10% [15]. These values of two shift mean that there was any misassemble or mechanical defect during the sinusoidal vibration test.

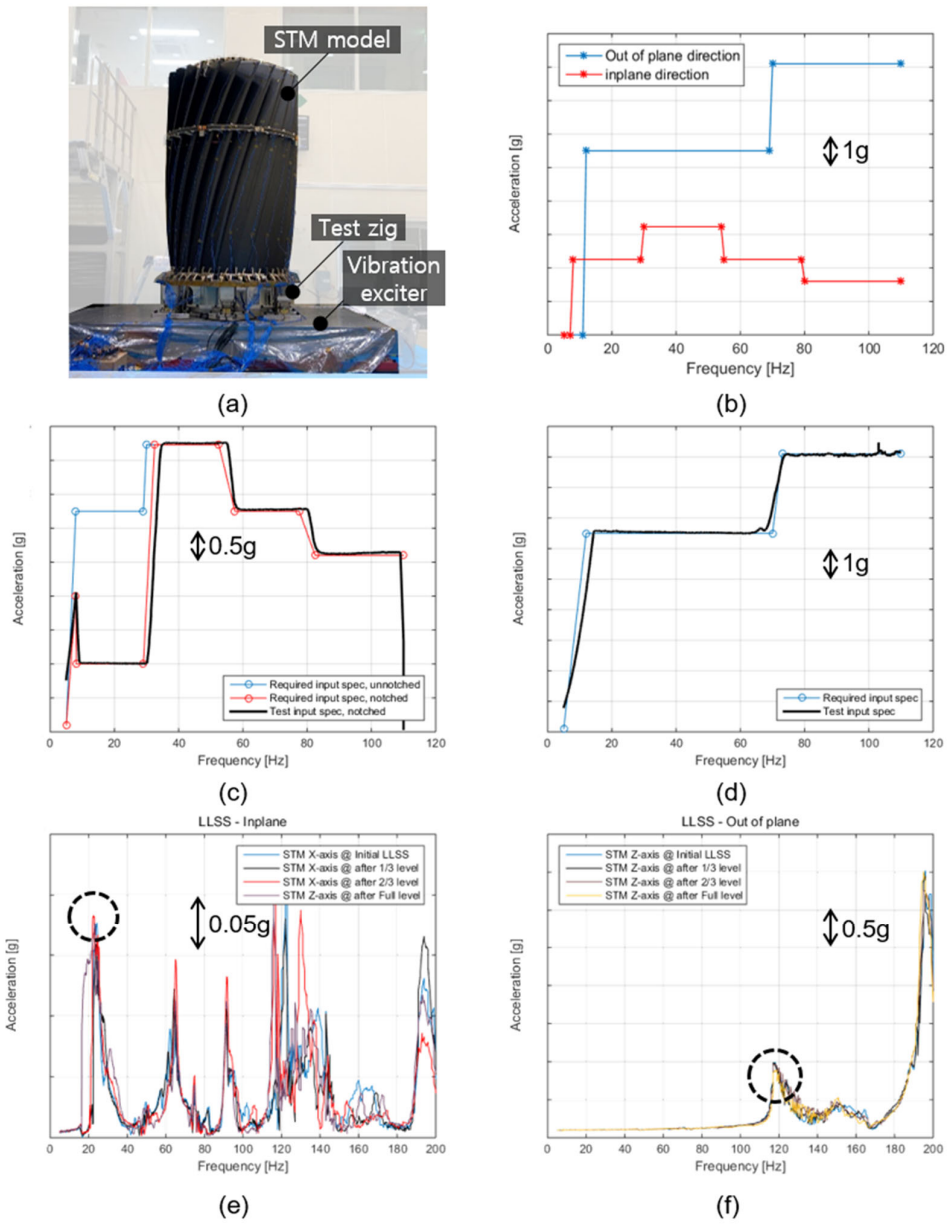


Figure 5. Sinusoidal vibration test; (**a**) test setup for the inplane direction; (**b**) required environmental test specification; the test specifications for (**c**) inplane and (**d**) out-of-plane directions; the result of the low-level sine sweep (LLSS) for (**e**) inplane and (**f**) out-of-plane directions; The frequency and amplitude at the peak frequency of dashed circle in (**e**,**f**) are used for the reference of the modal survey.

Table 1. Required specification of sinusoidal vibration test.

In-Plane Specification			Out-of-Plane Specification		
Frequency	**Acceleration**	**Tolerance**	**Frequency**	**Acceleration**	**Tolerance**
5–8 Hz	±0.00 mm	±3 dB	5–12 Hz	±0.00 mm	±3 dB
8–30 Hz	0.00 g	±3 dB	12–70 Hz	0.00 g	±3 dB
30–55 Hz	0.00 g	±3 dB	70–110 Hz	0.00 g	±3 dB
55–80 Hz	0.00 g	±3 dB			
80–110 Hz	0.00 g	±3 dB			
Maximum acceleration: 9 g or more			Maximum acceleration: 4 g or more		

4. Acoustic Loading Test of the Deployable Reflector Antenna in STM Phase

Figure 6 shows the test configuration and procedure of the acoustic load test in STM phase. The acoustic load test is a test to evaluate the structural integrity of the satellite or payload against the high-level reverberation field formed inside the launch vehicle fairing during the launch process. To mimic the reverberation field generated inside the launch vehicle fairing, a high sound pressure is created in the reverberation room environment using an acoustic modulator. The required specification of the acoustic load test defined in Table 2 can be realized by feedback control by several control microphones. As mentioned in Section 2, the acoustic load test is performed with −4 dB level of required specification before the full level test to protect the test sample and prevent damage to the equipment. The acoustic load test is conducted in two stages, and a low-level acoustic random test (LLART) is performed with −8 dB level of the original specification before/after each test as shown in Figure 6b. The pass/fail of the acoustic load test is determined by calculating the frequency and amplitude shift of the fundamental mode frequency caused by the acoustic load through the LLART. Similar with the sinusoidal vibration test, if the frequency and amplitude shift of the fundamental mode is more than 5% before/after each test, it is considered that there is a problem with the test specimen [15].

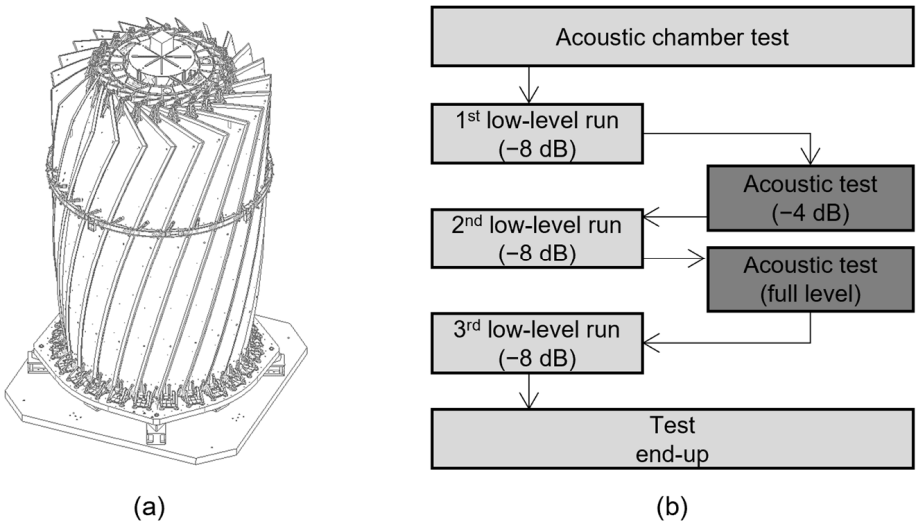


Figure 6. Concept of the acoustic load test; (**a**) Test configuration with the acoustic zig; (**b**) Test procedure.

Table 2. Required specification of the acoustic load test.

Center Frequency (1/1 Octave Band)	Sound Pressure Level	Tolerance
31.5	0.00 dB	−2 dB/+4 dB
63	0.00 dB	−1 dB/+3 dB
125	0.00 dB	−1 dB/+3 dB
250	0.00 dB	−1 dB/+3 dB
500	0.00 dB	−1 dB/+3 dB
1000	0.00 dB	−1 dB/+3 dB
2000	0.00 dB	−1 dB/+3 dB
4000	0.00 dB	N/A
8000	0.00 dB	N/A
OASPL	144 dB or more	−1 dB/+3 dB
Duration: 2 min		

However, since it is difficult to control the sound pressure level (SPL) in the high-frequency range, there is any tolerance requirement of the SPL in the 4000–8000 Hz frequency band. Therefore, pass/fail of the acoustic load test is determined by not only SPL within the frequency band of 31.5~2000 Hz but also the overall sound pressure level (OASPL). In the acoustic load test conducted in this study, the sound pressure level used in the test was measured by the reference microphone as shown in Figure 7a. As shown in Figure 7b, the acoustic load test satisfies the test tolerance in the frequency range of 31.5–2000 Hz, and the measured OASPL showed an output that was 0.35 dB higher than the sound pressure level of the required specification. As shown in Figure 7c, the results of LLART before/after the full-level acoustic load test show a frequency shift of less than 5% and an amplitude shift of less than 10% [15].

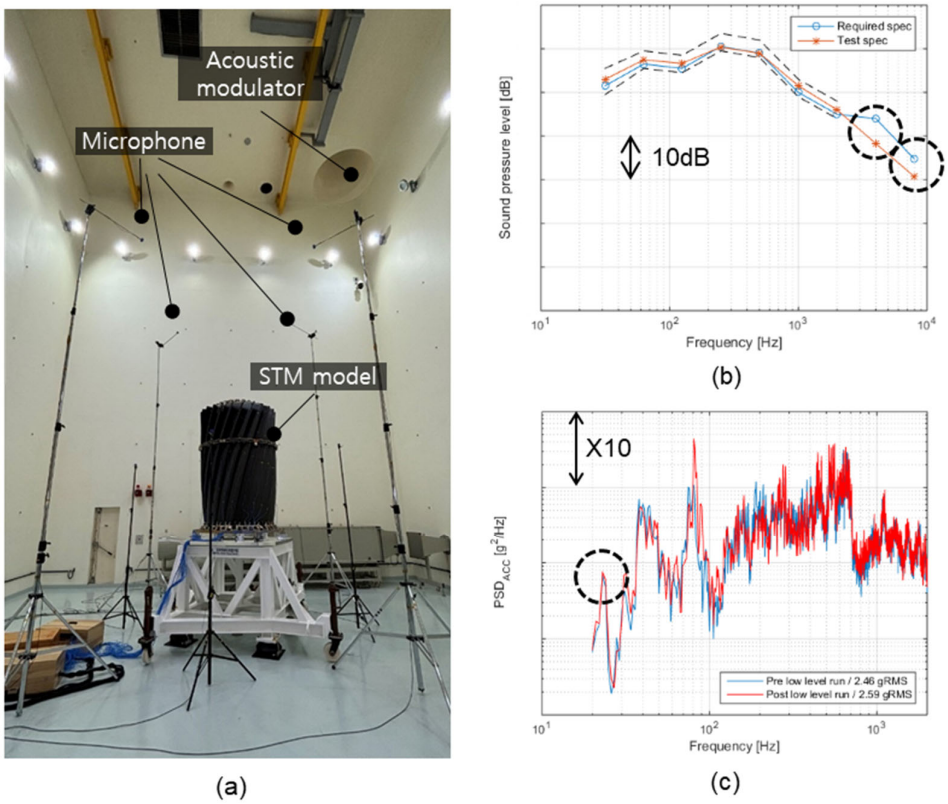


Figure 7. Acoustic load test; (**a**) the required environmental specification and the measured sound pressure level; (**b**) the result of the low-level acoustic random test before and after acoustic load test of the full level; There is no tolerance guideline in the high frequency range for the center frequency of 4 k, 8 kHz (black dashed circle in subfigure (**b**)); (**c**) the result of the low level acoustic random test before/after the acoustic load test; The frequency and amplitude at the 1st peak frequency is used for the reference of the modal survey (black dashed circle in (**c**)).

5. Thermal Balance Test of the Deployable Reflector Antenna in STM Phase

This section deals with the results of the thermal balance test of the STM of the deployable reflector antenna. The thermal balance test of the reflector antenna was conducted in the Dirty Thermal Vacuum Chamber of the Korea Institute of Construction Technology (KICT). This chamber is a lunar surface environment simulator for various tests on the construction environment on the lunar surface, and we decided to use this equipment because the thermal balance test in STM phase does not have any requirement for cleanliness of test facilities. To develop a satellite antenna, a thermal analysis should be performed to evaluate the temperature range of the antenna for the orbital thermal environment and to

confirm the thermal stability. To construct the reliable thermal analysis model, the optical properties of the reflector antenna components and the thermal conductivity coefficient between the assembly interfaces should be correlated. First of all, the thermal analysis model is constructed based on the general optical properties and thermal conductivity coefficients. Using this thermal analysis model, thermal analysis of the ground test is numerically performed, and then numerical optimization is performed using the temperature data measured in the thermal balance test. By using numerical optimization to minimize the difference between the temperature data obtained from the test and the results of the thermal analysis, a well-correlated thermal model is constructed. For the model correlation, we use the thermal desktop® which is thermal analysis software in Ansys 2023 R2. In this program, the error between the numerically computed and experimentally measured temperature data of each component is minimized based on the reduced order modeling. Using the reduced-order model, computational cost is efficiently reduced, and the reliability of the thermal analysis mode is improved [16,17]. Figure 8 shows the test configuration and procedure of the thermal balance test to measure the temperature data used for the model correlation.

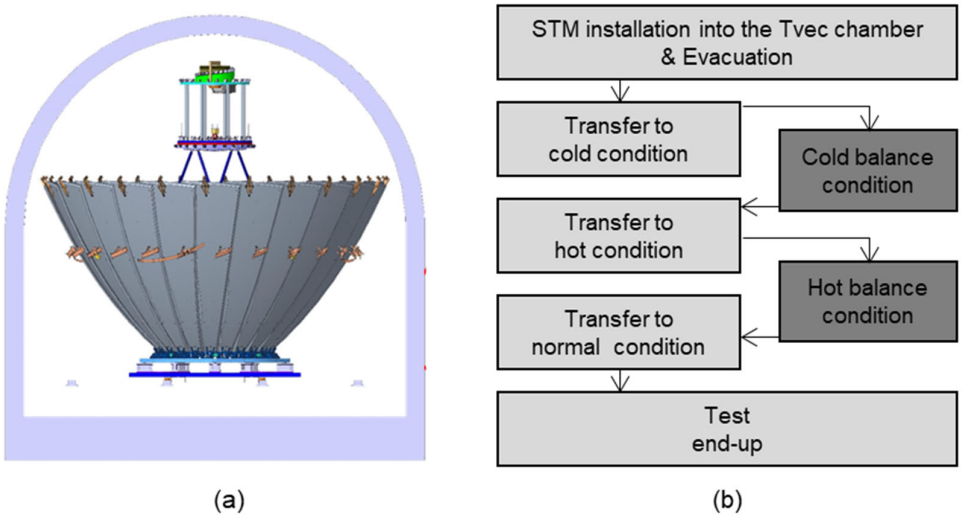


Figure 8. Concept of the thermal balance test; (**a**) Test configuration with thermal vacuum chamber; (**b**) test procedure.

Figure 9 shows the test configuration and the time history of shroud temperature and vacuum pressure during the thermal balance test. As shown in Figure 9a, the STM of the reflector antenna was located in the center of thermal vacuum chamber with a semi-deployed condition during the thermal balance test. Since the temperature data measured by the thermal balance test is used as the reference data for correlating the optical properties and the thermal conductivity of the thermal model for the ground test simulation, it is important to measure the thermal distribution with a clear temperature difference in the cold/hot balance condition. To impose the clearly deferent thermal source, the patch heaters were attached to three of the 24-unit main reflectors, as shown in Figure 9b. For the cold/hot balance conditions, three main reflectors are powered by 550 W and 1650 W respectively. As shown in Figure 9c,d, the thermal equilibrium tests were conducted in a thermal vacuum chamber with the vacuum pressure lower than 1^{-6} torr and shroud temperature lower than -196 °C, respectively. Except for Phase III that the test was briefly paused, the vacuum pressure and shroud temperature satisfy the test requirements. The temperature data for cold/hot balance condition measured by the thermal balance test will be used to construct a reliable thermal analysis model. In QM, using the well-correlated thermal analysis model, the orbital thermal analysis will be conducted to define the operational temperature range.

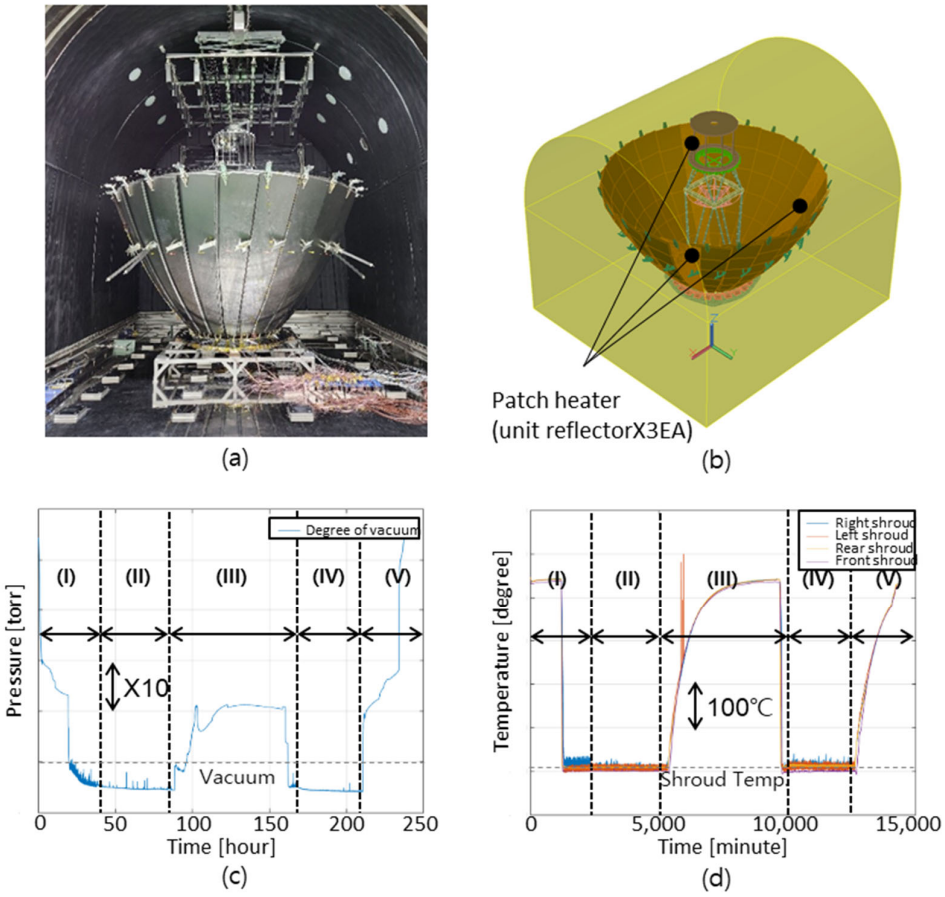


Figure 9. Result of the thermal balance test; (**a**) the test configuration of the thermal balance test; (**b**) thermal mathematical model (TMM) with three patch heaters; the time history of (**c**) vacuum pressure and (**d**) shroud temperature within the duration of test consisting of I. the evacuation and transient phase into the cold condition II. the cold balance condition; III. the break time without test and transient phase into the hot condition, IV. the hot balance condition and V. the transient phase into the ambient condition.

6. Conclusions

In this paper, we performed environmental tests on the deployable reflector antenna, which is the core payload of the SAR satellite, in STM phase. The environmental tests of the deployable reflector antenna are divided into structural tests to simulate the launch environment and thermal tests to simulate the orbital environment. The structural tests of the STM phase are divided into sinusoidal vibration and acoustic load tests to verify the structural stability for the launch process at the qualification level. The thermal balance tests to verify the thermal stability under the cold/hot balance conditions and obtain the temperature data for the correlation of the thermal analysis model. During each test, visual inspection was performed to check for damage to the specimen before/after each test. A series of low-level sine sweep test and low-level acoustic random test were performed to calculate the frequency and amplitude shift of the fundamental modes in each direction, during each test. Using these environmental tests, the structural/thermal stability of the deployable reflector antenna could be verified with respect to the environment specification. The result of environmental tests conducted at STM Phase will be applied to the correlation of structural/thermal analysis models to design and manufacture the qualification models of the deployable reflector antennas.

Author Contributions: Conceptualization, Y.Y.; methodology, D.-G.K.; software, H.-G.K. and D.-G.K.; validation, M.-J.K., H.-G.K., R.-H.D. and D.-G.K.; formal analysis, D.-G.K.; investigation, H.-G.K.; resources, R.-H.D. and Y.Y.; data curation, D.-G.K.; writing—original draft preparation, H.-G.K., R.-H.D. and D.-G.K.; writing—review and editing, M.-J.K. and K.-R.K.; visualization, H.-G.K.; supervision, K.-R.K.; project administration K.-R.K.; funding acquisition, K.-R.K. All authors have read and agreed to the published version of the manuscript.

Funding: This study was conducted with support from the Korea Research Institute for defense Technology planning and advancement and the Defense Acquisition Program Administration in 2021 (20-207-B00-011-001).

Institutional Review Board Statement: Not applicable.

Informed Consent Statement: Not applicable.

Data Availability Statement: The original contributions presented in the study are included in the article, further inquiries can be directed to the corresponding author.

Conflicts of Interest: Authors Hyun-Guk Kim, Dong-Geon Kim, Ryoon-Ho Do, Min-Ju Kwak, Kyung-Rae Koo and Youngjoon Yu were employed by the company Hanwha Systems. All authors declare that the research was conducted in the absence of any commercial or financial relationships that could be construed as a potential conflict of interest.

References

1. Urata, K.N.; Sumantyo, J.T.S.; Santosa, C.E.; Viscor, T. Development of an L-band SAR microsatellite antenna for earth observation. *Aerospace* **2018**, *5*, 128. [CrossRef]
2. Moreira, A.; Prats-Iraola, P.; Younis, M.; Krieger, G.; Hajnsek, I.; Papathanassiou, K.P. A tutorial on synthetic aperture radar. *IEEE Geosci. Remote Sens. Mag.* **2013**, *1*, 6–43. [CrossRef]
3. Gao, G.; Yao, L.; Li, W.; Zhang, L.; Zhang, M. Onboard information fusion for multisatellite collaborative observation: Summary, challenges, and perspectives. *IEEE Geosci. Remote Sens. Mag.* **2023**, *11*, 40–59. [CrossRef]
4. Pappas, O.; Biggs, J.; Prats-Iraola, P.; Pulella, A.; Stinton, A.; Achim, A. Measuring topographic change after volcanic eruptions using multistatic SAR satellites: Simulations in preparation for ESA's Harmony mission. *Remote Sens. Environ.* **2025**, *317*, 114528. [CrossRef]
5. Cutrona, L.-J. Synthetic aperture radar. *Radar Handb.* **1990**, *2*, 2333–2346.
6. Kim, H.-G.; Kim, D.-G.; Do, R.-H.; Koo, K.-R.; Yu, Y. Development of Deployable Reflector Antenna for the SAR-Satellite: Part 1. Design and Analysis of the Main Reflector using Honeycomb Sandwich Composite Structure. *Appl. Sci.* **2024**, *14*, 1590. [CrossRef]
7. Meguro, A.; Harada, H.; Watanabe, M. Key technologies for high-accuracy large mesh antenna reflectors. *Acta Astronaut.* **2003**, *53*, 899–908. [CrossRef]
8. Sun, Z.; Yang, D.; Duan, B.; Kong, L.; Zhang, Y. Structural design, dynamic analysis, and verification test of a novel double-ring deployable truss for mesh antennas. *Mech. Mach. Theory* **2021**, *165*, 104416. [CrossRef]
9. Thomson, M.-W. The AstroMesh deployable reflector. In Proceedings of the IEEE Antennas and Propagation Society International Symposium. 1999 Digest. Held in conjunction with: USNC/URSI National Radio Science Meeting (Cat. No.99CH37010), Orlando, FL, USA, 11–16 July 1999.
10. Xiao, B.; Yin, S.; Wu, L. A structure simple controller for satellite attitude tracking maneuver. *IEEE Trans. Ind. Electron.* **2016**, *64*, 1436–1446. [CrossRef]
11. Snyder, J.-F.; Wong, E.-L.; Hubbard, C.-W. Evaluation of commercially available carbon fibers, fabrics, and papers for potential use in multifunctional energy storage applications. *J. Electrochem. Soc.* **2009**, *156*, A215. [CrossRef]
12. EURO-COMPOSITES. "Mechanical Properties of ECK Honeycomb". 2010. Available online: https://www.nzcomposites.com/site/nzcomposites/ECK%20Honeycomb%20Properties.pdf (accessed on 24 November 2024).
13. Kim, D.-G.; Kim, H.-G.; Kim, D.-Y.; Do, R.-H.; Koo, K.-R.; Yu, Y. Development of a Deployable Reflector Antenna for the Synthetic Aperture Radar Satellite, Part 2: Manufacturing and Qualification of the Main Reflector Using a Honeycomb Sandwich Composite Structure. *Appl. Sci.* **2024**, *14*, 11273. [CrossRef]
14. Kistler. *Instruction Manual: 3-Component Force Link Type 9377C*; Kistler Group: Winterthur, Switzerland, 2009.
15. Kim, H.-G.; Kwon, S.-C.; Koo, K.-R.; Song, S.-C.; Yu, Y.; Song, T.; Park, Y.H.; Oh, H.-U. Performance Investigation of Superplastic Shape Memory Alloy-Based Vibration Isolator for X-Band Active Small SAR Satellite of S-STEP under Acoustic and Random Vibration Environments. *Aerospace* **2022**, *9*, 6645. [CrossRef]

16. Hegeveld, D.-W.; Biskner, A. Enhanced data exploration through Reduced-order models. In Proceedings of the 47th International Conference on Environmental Systems, Charleston, SC, USA, 16–20 July 2017.
17. Shibukawa, T.; Nakasuka, S. A System-Level Thermal Model Reduction Method Applicable to Transient analysis. In Proceedings of the 52th international Conference on Environmental Systems, Calgary, AB, Canada, 16–20 July 2023.

Disclaimer/Publisher's Note: The statements, opinions and data contained in all publications are solely those of the individual author(s) and contributor(s) and not of MDPI and/or the editor(s). MDPI and/or the editor(s) disclaim responsibility for any injury to people or property resulting from any ideas, methods, instructions or products referred to in the content.